

# Mechanism of Cr(III)-based oxide-hydroxide film electrodeposition in an acidic solution

Sharifi, Z.; Behjati, S.; Wijenberg, J.H.O.J.; Vooys, A.C.A. de; Koper, M.T.M.

# Citation

Sharifi, Z., Behjati, S., Wijenberg, J. H. O. J., Vooys, A. C. A. de, & Koper, M. T. M. (2024). Mechanism of Cr(III)-based oxide-hydroxide film electrodeposition in an acidic solution. *Electrochimica Acta*, *512*. doi:10.1016/j.electacta.2024.145451

Version: Publisher's Version

License: <u>Creative Commons CC BY 4.0 license</u>
Downloaded from: <u>https://hdl.handle.net/1887/4283098</u>

**Note:** To cite this publication please use the final published version (if applicable).

Contents lists available at ScienceDirect

# Electrochimica Acta

journal homepage: www.journals.elsevier.com/electrochimica-acta





# Mechanism of Cr(III)-based oxide-hydroxide film electrodeposition in an acidic solution

Zahra Sharifi <sup>a</sup>, Saeid Behjati <sup>a</sup>, Jacques H.O.J. Wijenberg <sup>b</sup>, Arnoud C.A. de Vooys <sup>b</sup>, Marc T.M. Koper <sup>a,\*</sup>

#### ARTICLE INFO

Keywords: Cr(III) coatings Local pH EQCM EC-STM

#### ABSTRACT

The electrodeposition of chromium oxide-hydroxide films from Cr(III) electrolytes has recently become a significant focus in electrochemistry, holding promise for applications in packaging industry and corrosion protection, as an environmentally friendly alternative for Cr(VI). However, the complex behavior of Cr(III) complexes has resulted in a scarcity of precise electrochemical investigations in this field. In this study, we employ in-situ techniques such as Electrochemical Quartz Crystal Microbalance (EQCM) and Electrochemical Scanning Tunneling Microscopy (EC-STM) in conjunction with cyclic voltammetry (CV) to elucidate the mechanisms governing the formation of chromium oxide-hydroxide films through electrodeposition in an acidic environment. CV studies explore the electrochemical reactions involved in the electrodeposition process, showing that hydrogen evolution is the dominant reaction. The resulting interfacial pH changes trigger the hydrolysis of hydrated chromium(III) cations, leading to oligomerization and the precipitation of a chromium hydroxide compound. In-situ monitoring of mass changes during film formation process using EQCM reveals that there is a critical pH range for oxide-hydroxide film formation, outside of which no deposition/precipitation occurs. EC-STM results confirms the formation of a film on the cathode surface, and its sensitivity to the interfacial pH. At a sufficiently high local pH, under our experimental conditions happening at potentials more negative than -0.95 V, the film alters into a state that becomes stable and insoluble.

#### 1. Introduction

Over the past decades, extensive research has been conducted on the development of chromium coatings for various industries such as automotive, packaging, aerospace, defense, and military. Among the primary technologies utilized in the production of chromium coatings is electrodeposition from hexavalent chromium (Cr(VI)) baths. Chromium coatings electroplated from Cr(VI) baths exhibit excellent properties such as high hardness, wear resistance, corrosion resistance, adhesion, and coverage. However, the inherent toxicity and carcinogenicity associated with Cr(VI) ions, coupled with the regulatory measures imposed by the European Union under the framework of REACH (Registration, Evaluation, Authorization, and Restriction of Chemicals) to limit their usage, have motivated researchers to explore alternative systems based on more environmentally friendly alternatives like trivalent chromium ions (Cr(III)). Cr(III)-based electroplating baths exhibit significantly lower environmental hazards compared to their Cr

(VI) counterparts, however the Cr(III) baths have lower conductivity and poorer covering power, leading to slower deposition rates and reduced efficiency. Additionally, the process often requires extra chemicals or co-deposition techniques, complicating the plating process compared to Cr(VI) baths [1,2]. To increase the efficiency of the process and enhance the coating quality, extensive efforts have been made to understand the behavior of Cr(III) ions during electrodeposition and to elucidate the mechanism of this process. Understanding the intricate mechanisms and behaviors of chromium(III) complexes holds the promise of refining trivalent chromium-based plating systems, thereby eliminating the necessity for hexavalent chromium and mitigating associated hazards.

Given the complexity inherent in the behavior of trivalent chromium species, conclusive mechanisms for the electrodeposition of chromium from trivalent chromium baths have not yet emerged. Existing literature has focused on the formation of metallic chromium and in general outlines a two-stage mechanism for the reduction of chromium (III) to

E-mail address: m.koper@chem.leidenuniv.nl (M.T.M. Koper).

<sup>&</sup>lt;sup>a</sup> Leiden Institute of Chemistry, Leiden University, P.O. Box 9502, Leiden, 2300 RA, the Netherlands

<sup>&</sup>lt;sup>b</sup> Tata Steel, Research & Development, IJmuiden Technology Centre, P.O. Box 10.000, IJmuiden, 1970 CA, the Netherlands

<sup>\*</sup> Corresponding author.

metallic chromium and assume that the first electron transfer is the rate determining step [3,4]. The first step is the initial reduction of trivalent chromium species to divalent chromium (Reaction 1), both in solution (sol), and the second step is further reduction of divalent chromium to metallic chromium (Reaction 2).

$$Cr^{3+}(sol) + e^{-} \rightarrow Cr^{2+}(sol)$$
 (1)

$$Cr^{2+}(sol) + 2e^{-} \rightarrow Cr(s)$$
 (2)

In aqueous systems at acidic pH, the reduction of trivalent chromium takes place at relatively negative potential, concurrent with proton and water reduction reactions, leading to local pH elevation near the electrode surface [5,6] due to Reaction 3a and 3b.

$$2H_3O^+ + 2e^- \rightleftharpoons H_2 + 2H_2O$$
 (3a)

$$2H_2O + 2e^- \rightleftharpoons H_2 + 2OH^-$$
 (3b)

In the presence of a bridging ligand with a basic lone pair, like hydroxide (OH<sup>-</sup>), the trivalent chromium ions become oligomerized and exist in various complex species—mononuclear, binuclear, trinuclear, and beyond—each characterized by differing charges determined by the number of ligands within the complex [7]. Near the electrode surface. these species can subsequently undergo further reduction or deposit on the surface as insoluble di/trivalent chromium hydroxides [8,9]. Wijenberg et al. showed that in the presence of formate ions and under conditions of high mass transport using a rotating cylinder electrode, an increase in local pH on the electrode surface leads to the deprotonation of the water molecule ligands in Cr(III) complexes. At current densities below 20 A/dm<sup>2</sup>, the local pH increase is minimal, forming soluble Cr (III) species without deposition (Reaction 4). Between 20 and 45 A/dm<sup>2</sup>, the local pH increase is higher, leading to the deposition of insoluble Cr (III) species (Reaction 5). Part of this deposit is further reduced to metallic chromium, while the rest forms chromium carbide and chromium oxide. At current densities above 45 A/dm<sup>2</sup>, the local pH reaches its maximum, resulting in the dissolution of the deposited layer and the formation of insoluble anionic complexes, which are mainly chromium oxides (Reaction 6) [10].

$$[Cr(HCOO)(H_2O)_5]^{2+} + OH^- \rightleftharpoons [Cr(HCOO)(OH)(H_2O)_4]^+ + H_2O$$
 (4)

$${\rm [Cr(HCOO)(OH)(H_2O)_4]}^+ + {\rm OH}^- \! \rightleftharpoons \! {\rm [Cr(HCOO)(OH)_2(H_2O)_3]}^0 + {\rm H_2O}$$
 (5)

$$[{\rm Cr}({\rm HCOO})({\rm OH})_2({\rm H_2O})_3]^0 + {\rm OH}^- {\rightleftharpoons} [{\rm Cr}({\rm HCOO})({\rm OH})_3({\rm H_2O})_2]^- + {\rm H_2O} \end{(6)}$$

Danilov et al. proposed a four-stage reduction process, wherein trivalent chromium initially converts to divalent chromium (Reaction 7) and then due to the local pH increase to divalent chromium hydroxide (Reaction 8), followed by the second electron transfer and subsequent deposition of monovalent chromium hydroxide (Reaction 9), which then transforms into metallic chromium (Reaction 10) [11].

$$Cr(III)L^{(3+n)}_{S} + e^{-} \rightleftharpoons Cr(II)L^{(2+n)}_{S}$$
(7)

$$Cr(II)L^{(2+n)}_{S} + OH_{S}^{-} \rightleftharpoons Cr(II)OH^{(+)}_{S} + L^{n}_{S}$$
(8)

$$Cr(II)OH_S^+ + e^- \rightleftharpoons Cr(I)OH_S$$
 (9)

$$Cr(I)OH_S + e^- \rightleftharpoons Cr(0) + OH_S^-$$
(10)

In these reactions, L is a ligand, n is charge of the ligand and S indicates that the reaction takes place near the electrode surface. Danilov et al. claimed that the electrodeposition of chromium occurs via an inner-sphere bridge mechanism, involving the participation of hydroxocomplexes containing divalent chromium.

In another study, Protsenko et al. demonstrated, based on mathe-

matical simulations, that the choice of ligand can influence the reduction mechanism. For instance, in the presence of formate anions, trivalent chromium is first reduced to divalent chromium hydroxide, subsequently transforming into metallic chromium upon the transfer of two electrons and two protons (Reactions 11 and 12) [12].

$$\begin{split} & \left[ \text{Cr(II)(HCOO}^{-})_m (\text{H}_2\text{O})_n \right]_{\text{ads}} \\ & \quad \leftrightarrow \left[ \text{Cr(II)(HCOO}^{-})_{m-k} (\text{H}_2\text{O})_{n-1} (\text{OH})^{-} \right]_{\text{ads}} \\ & \quad + k \text{HCOO}^{-} + \text{H}^{+} \end{split}$$

(11)

$$\begin{split} & \left[ \text{Cr(II)(HCOO}^{-})_{\text{m-k}} (\text{H}_{2}\text{O})_{\text{n-1}} (\text{OH})^{-} \right]_{\text{ads}} + 2\text{H}^{+} + 2\text{e}^{-} \leftrightarrow \text{Cr}^{0} \\ & + (m-k)\text{HCOO}^{-} + \text{nH}_{2}\text{O} \end{split} \tag{12}$$

where m = 1,2; k = 0,1,2.

Conversely, in the presence of oxalate, the second and third electron transfers occur immediately after the first electron transfer (Reaction 13)

$$[Cr(II)(COO^{-})_{2}(H_{2}O)_{n}]_{ads} + 2H^{+} + 2e^{-} \leftrightarrow Cr^{0} + (COOH)_{2} + nH_{2}O$$
 (13)

The questions of whether trivalent chromium ions are first reduced to divalent chromium in a two-step process before precipitating, whether they precipitate in a three-step process with the transfer of one electron at each stage, and whether they are initially adsorbed on the surface as hydroxide before the reduction steps occur, have remained elusive. As stated before, current literature has focused on the formation of metallic chromium, and assume that the first electron transfer is the rate determining step. However, the chromium (III) hexaqua complex is known to be a Bronsted acid and chromium hydroxides are known to be poorly soluble, suggesting that deprotonation reactions could be equally important in the generation of the final deposit [10]. A first step to elucidate the mechanism is to exclude the effects of complexing agents on the aqueous chromium chemistry, that is to study the system in the absence of any added complexing anions. It has been established that these conditions will result in an oxidic deposit. This deposit is in fact of practical interest, as it functions as an adhesion/passivation promotor for industrially relevant coatings. Prabhakar et al. have demonstrated that the deposit is an amorphous layer with a mixture of Cr<sup>2+</sup> and Cr<sup>3+</sup> oxyhydroxides [13]. The amorphous nature of the deposition suggests that it does not follow a classical nucleation & growth-type mechanism, highlighting the necessity of establishing the initial stages of film formation [13,14]. Furthermore, in nearly all the research conducted thus far on trivalent chromium reduction, in situ measurements have been quite limited. Considering the complexity of the chemistry of trivalent chromium species and their sensitivity to air and dehydration, employing techniques capable of investigating the state of the surface in situ is essential for obtaining more precise and reliable results. Such methodologies can complement electrochemical approaches, making the elucidation of the mechanisms governing the behavior of Cr(III) species during electrodeposition more reliable. Accordingly, this study aims to investigate the electrochemical behavior of Cr(III) complexes near the cathode surface utilizing in-situ methodologies, specifically Electrochemical Quartz Crystal Microbalance (EQCM) and Electrochemical Scanning Tunneling Microscopy (EC-STM). Our focus will be on specifying the step by step mechanism that leads to the formation of Cr(III) oxy-hydroxide film during electrodeposition from acidic aqueous solution.

#### 2. Experimental section

#### 2.1. Chemicals

The chemicals used were Milli-Q water (for both preparing chemical solutions and cleaning, resistivity  $>18.2~\text{M}\Omega\cdot\text{cm}$ , TOC <5~ppb),  $\text{H}_2\text{SO}_4$  (96 % ultrapure, Merck), HClO $_4$  (60 %, Merck – EMSURE ACS), Na $_2\text{SO}_4$  (99.995 % metal basis, Alfa Aesar), sodium perchlorate hydrate (99.99

% trace metal basis, Merck, NaOH(30 % solution, Suprapur, Merck),  $H_2O_2(35$  %,Merck), basic chromium(III) sulphate (BCS) salt ((CrOH-SO<sub>4</sub>)<sub>2</sub>Na<sub>2</sub>SO<sub>4</sub>  $\times$  H<sub>2</sub>O) with trade name Trisurfin® .

#### 2.2. General electrochemical procedure

All electrochemical experiments were conducted with a borosilicate glass cell, which was custom-designed and manufactured by the Leiden Instrumentmakers School (LIS). This specialized cell is equipped with four ports designated for the working, counter, and reference electrodes, as well as two ports for gas introduction and outlet. Additionally, a Luggin capillary separates the reference electrode from the cell. The process of cleaning glassware involves three sequential steps:

- 1. Initially, all glassware was immersed in a solution containing  $H_2SO_4$  (0.5 M) and  $KMnO_4$  (6mM) for a minimum of 12 h.
- 2. Following this soaking, the glassware was thoroughly rinsed with water and subsequently placed in a diluted piranha solution for a duration of 10 min. This step served to eliminate any potential residues of  $MnO_4$  and  $MnO_2$  impurities.
- Lastly, the glassware underwent a thorough rinsing process and was boiled in water, repeating this cycle at least four times.

The reference electrode was a reversible hydrogen electrode (RHE, Gaskatel, HydroFlex). The counter electrode was a gold wire (high purity, 99.999 %) and the working electrode was a polycrystalline gold bead electrode with a semi-spherical shape, having an approximate surface diameter of 2.5 mm, held in hanging meniscus configuration. The counter electrode was ca. 1 cm from the working electrode and was not separated from the rest of the cell by a membrane. Cyclic voltammetry experiments were conducted using a 4-channel Biologic potentiostat (VSP-300).

The preparation of the working electrode involved five steps, all of which are performed before each measurement:

- 1. Electrochemical oxidation and acid cleaning: This process entails oxidizing the electrode surface in a 0.1 M sulfuric acid solution by applying a 10 V voltage for 20 s. A graphite bar serves as the counter electrode during this step. Subsequently, any formed gold oxide is removed by immersing the working electrode in a 6 M HCl solution for 30 s.
- 2. Mechanical polishing: The electrode is then mechanically polished using a polishing machine. It is rinsed and successively polished with 3  $\mu$ m, 1  $\mu$ m, 0.25  $\mu$ m, and 0.05  $\mu$ m diamond suspensions (MetaDi, Buehler), each for a duration of 2 min.
- 3. Ultrasonic cleaning: To eliminate any potential residues from the mechanical polishing on the electrode surface, the electrode is subjected to ultrasonic cleaning in water for 2 min.
- 4. Flame annealing and quenching: To eliminate organic contaminants, residual oils, or any other impurities present on the electrode's surface, the electrode surface was annealed. Additionally, this process aimed to alleviate any residual stresses that might have been induced during mechanical polishing. The electrode underwent flame annealing for a few seconds and was then promptly quenched in water. This cycle was repeated ten times.
- 5. Electropolishing and surface characterization: The final step involves electropolishing and the characterization of the surface. Electropolishing is accomplished by cycling the electrode through 200 cycles between 0 and 1.65 V at a scan rate of 1 V/s in a 0.1 M H<sub>2</sub>SO<sub>4</sub> solution. Additionally, before each measurement, cyclic voltammetry of the gold surface is performed within a potential range of 0 to 1.65 V at a scan rate of 50 mV/s (Figure S1). This step is crucial for evaluating both the quality and cleanliness of the electrode surface and the solution. Furthermore, we use the characteristic cyclic voltammogram of gold to determine the electrochemical surface area (ECSA) of the electrode. This is achieved by calculating the ratio of

the charge associated with the reduction peak of Au oxide to the charge density of a monolayer of Au oxide (386  $\mu$ C cm<sup>-2</sup>).

High-purity argon (6.0 purity, Linde) was purged through the solution for at least 20 min before the experiments began. Throughout the experiments, a continuous flow of argon was maintained over the solution to prevent the diffusion of oxygen into the electrolyte.

#### 2.3. EQCM

An Autolab EQCM module, in combination with the Metrohm Autolab PGSTAT series (12, 204, 128 N), was utilized to determine the electrode mass changes during the deposition of a chromium oxyhydroxide layer on a gold-coated EQCM crystal. The working electrode was a 6 MHz Au/TiO2 crystal electrode with a surface area of 0.35 cm<sup>2</sup> and a gold layer thickness of 200 nm, placed within a dedicated Autolab PEEK EQCM cell. The counter electrode was a gold wire, and the reference electrode was the RHE (mini-hydroflex). Argon gas was purged through the electrolyte for at least 30 min prior to each experiment. During the experiment the argon flow was turned off to prevent the vibration and noise it causes on the mass change detector. To minimize oxygen diffusion, the experiment were conducted quickly. Cyclic voltammetry tests were conducted at room temperature with a scan rate of 5 mV/s while simultaneously recording the quartz resonance frequency. The crystal's resonant frequency is highly sensitive to its total mass. The alteration in the oscillation frequency of the crystal  $(\Delta f)$  can be linked to the mass change of the crystal  $(\Delta m)$  using the Sauerbrey equation (Eq. (15)). By depositing a thin gold layer on the quartz crystal, the mass change of the gold-quartz crystal assembly can be monitored as a function of electrode potential, and changes in the measured mass must then be due to changes in the potential-induced processes at the surface of the gold electrode.

The frequency shift  $(\Delta f)$  observed on the EQCM analyzer is related to the mass change  $(\Delta m)$  of the quartz crystal-gold assembly  $(\Delta f_m)$  but also to the viscosity  $(\eta)$  and density  $(\rho)$  changes of the liquid adjacent to the quartz  $(\Delta f_{\eta\rho})$  (Eq. (14)). Given the minimal impact of the frequency shift resulting from the interaction between the aqueous solution and the quartz, our focus is primarily on the  $\Delta f_m$ .

$$\Delta f = \Delta f_m + \Delta f_{\eta\rho} \tag{14}$$

$$\Delta f = -\left(\frac{2f_0^2}{A\sqrt{\rho_q \mu_q}}\right) \Delta m \tag{15}$$

where  $\mu_q$  is the shear modulus of an AT-cut type quartz (2.947  $\times$   $10^{11} {\rm g/s.cm}$ ),  $\rho_q$  is quartz density (2.648  ${\rm g/cm^3}$ ), A is piezoelectric active area and  $f_0$  is the resonant frequency of the unloaded crystal (6 MHz) [15]. Frequency changes were converted into mass changes using the above equation, without additional experimental calibration. Since we do not know the exact composition of the film formed, nor can we derive it accurately from the experimental data, frequency and mass changes mainly serve a qualitative purpose, as well as the purpose of comparison between different experimental conditions.

### 2.4. In situ gas chromatography

In order to investigate the Faradaic efficiency of the hydrogen evolution reaction (HER) during the electrodeposition process from a 1 mM, 10 mM, and 100 mM  ${\rm Cr}^{3+}$  solutions at pH 2.5, gas chromatography was used. Experiments were conducted in a PEEK H-cell. The working electrode was a gold disk, and the counter electrode was a gold wire. The reference electrode was the RHE (mini-Hydroflex). The experiments were conducted at three potentials: -0.3 V, -0.5 V, and -0.75 V for 30 min of chronoamperometry in 1 mM, 10 mM, and 100 mM chromium solutions at pH 2.5. During the chronoamperometry, argon gas was continuously bubbled into the cell at a rate of 20 mL per minute. At 5,

20, and 30 min, a gas sample was taken online by a Shimadzu gas chromatograph and analyzed (these time intervals were selected based on the device limitations.) Based on the amount of hydrogen produced, the Faradaic efficiency of the hydrogen reduction reaction was calculated at the three potentials of -0.3 V, -0.5 V, and -0.75 V.

#### 2.5. EC-STM

A homebuilt electrochemical scanning tunneling microscopy (EC-STM) was used to capture topographical images after cyclic voltammetry at different potential windows (scan rate 0.05 Vs<sup>-1</sup>) [16]. The working electrode was a commercial Au(111) single crystal disc, placed face-up and the tip was hanging from the top which allows scanning of the surface in the electrolyte medium. The counter electrode was a gold wire, and the reference electrode was the RHE (mini-hydroflex). Prior to each experiment, the working and counter electrodes and the cell itself were thoroughly cleaned. The Au(111) single crystal was annealed to an orange color for 5 min and cooled down in air above a water surface. The cell components were soaked in the solution containing H<sub>2</sub>SO<sub>4</sub> (0.5 M) and KMnO<sub>4</sub> (6mM) for several hours and then in dilute piranha for about 30 min and finally rinsed and boiled in Milli-Q water five times. STM tips were made using the pull-cut method from a Pt/Ir wire and then coated with hot melt adhesive to minimize faradaic currents. All images were captured in constant current mode at 100-150 pA with a tunneling bias of -10 to -30 mV. The tip was retracted during the voltage sweep by setting the current setpoint to zero, and the tunneling current reappeared as the setpoint increased.

#### 3. Results and discussion

#### 3.1. Voltammetric measurements

We investigated the involvement of Cr(III) species in the electrode-position process of the formation of a chromium oxyhydroxide (Cr-O<sub>x</sub>-H<sub>x</sub>) film onto polycrystalline gold electrodes at room temperature by cyclic voltammetry (scan rate =0.005~V/s) with varying concentrations of Cr $^{3+}$  cations (0, 0.1, 1, 10, and 100 mM). The bulk pH was maintained at 2.5 across all solutions, by addition of perchloric acid after making the Cr(III) solution. Furthermore, 0.1 M sodium perchlorate solution was added to each solution to enhance conductivity.

Fig. 1 shows the cyclic voltammograms of the five solutions: Fig. 1a shows the full CVs, whereas Figs. 1b and 1c show zoomed-in versions of the negative- and positive-going scans, respectively. The lowest Faradaic current is observed in the solution without Cr<sup>3+</sup> (black curve in Fig. 1b), which must be due to proton reduction. In the presence of Cr3+, at concentrations higher than 1 mM, cathodic currents are significantly higher over the entire potential window, certainly in the negative-going scan. However, we consider that the current is still largely due to hydrogen evolution, and not to  ${\rm Cr}^{3+}$  reduction. First of all, the current does not scale linearly with Cr<sup>3+</sup> concentration. Secondly, based on Gas Chromatography (GC), the Faradaic Efficiency (FE) of H2 formation at potentials of -0.3, -0.5 and -0.75 V (region I, II and III in Fig. 1(b)) are  $95\pm38$  %,  $92\pm22$  % and  $95\pm13$  %, respectively. The FE for higher concentrations of Cr3+, 10 mM and 100 mM, at the same applied potentials were also higher than 90 % (with similar error bars) and do not depend on the Cr<sup>3+</sup> concentration. While this does not exclude some level of Cr<sup>3+</sup> reduction, it does mean that most of the current is due to hydrogen evolution. This is important as this leads to a corresponding local change in pH (see below). The Cr<sup>3+</sup>-induced enhancement of the HER leads to three observable features in the voltammogram, denoted regions I, II and III in Fig. 1(b). Region I is related to proton reduction (reactions 3a and 3b), and its current increases with Cr<sup>3+</sup> concentration because the Cr<sup>3+</sup> introduces an additional acid in solution through the  $\text{Cr}^{3+}(\text{H}_2\text{O})_6 \leftrightarrow \text{Cr}^{2+}(\text{H}_2\text{O})_5\text{OH} + \text{H}^+$  reaction, i.e. reaction 16 below. This acid-base reaction (proton donor) leads to an additional (proton) reduction current. [17]. The current peak in region II is very reminiscent

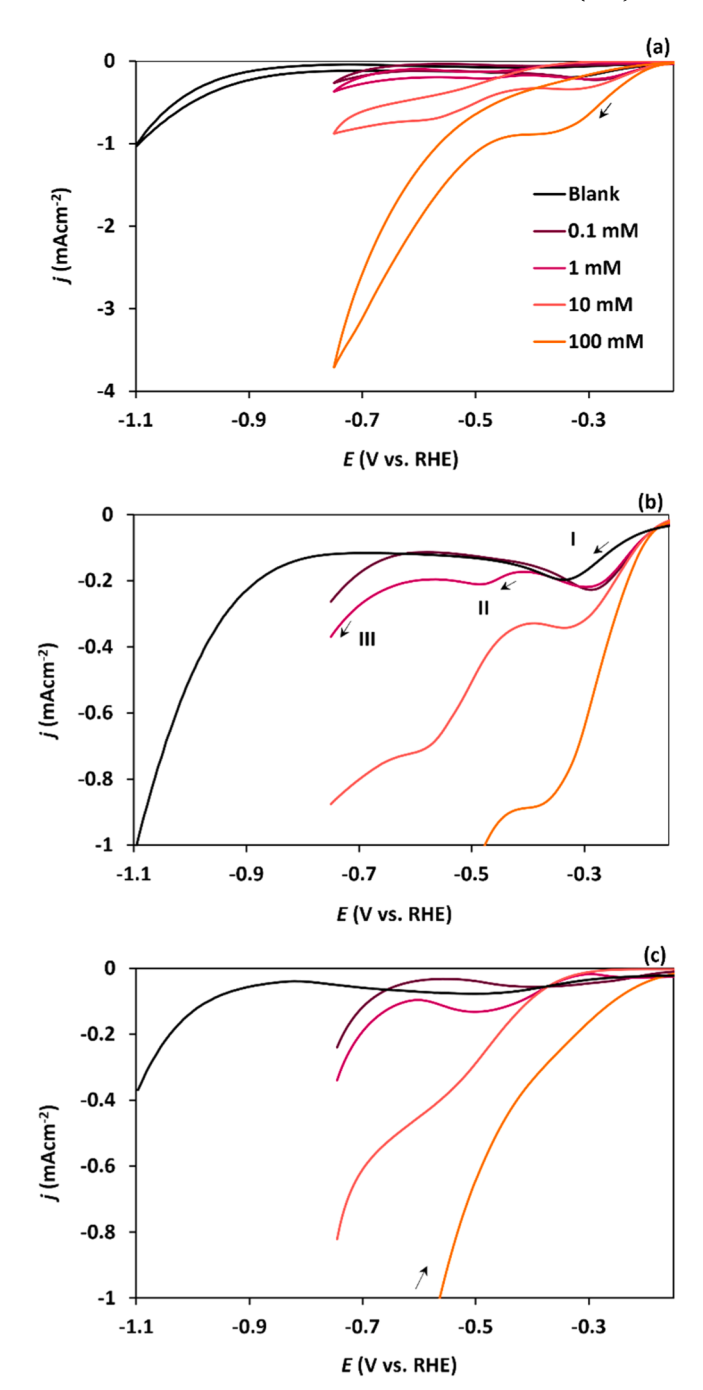


Fig. 1. a) Effect of  ${\rm Cr}^{3+}$  concentration (0.1 mM, 1 mM, 10 mM and 100 mM) on the cyclic voltammogram at a polycrystalline gold electrode (first cycle) b) negative-going scans c) positive-going scans (supporting electrolyte is 0.1 M NaClO4, pH = 2.5, scan rate 0.005 Vs<sup>-1</sup>).

of what has been observed for the effect of other multivalent cations on HER (see Fig. 3 in ref. [18]), and presumably related to a next acid-base equilibrium that generates protons at the corresponding interfacial pH, i.e. reaction 17 and 18 below. Finally, region III is ascribed to the enhancement by cations of the water reduction reaction (Reaction 3b), a reaction which is known to be very sensitive to the presence of cations in the electrolyte [19,20]. Moreover, it is observed that the current is generally lower in the return (positive-going) scan (Fig. 1c). This is likely partially due to mass transport effects, but also to the formation of a chromium-oxy-hydroxide layer on the gold surface (see next sections).

From the above interpretation of the CV, we conclude that a substantial interfacial pH increase must occur due to the various stages of

the HER [6]. As mentioned, this concentration polarization, in turn, triggers additional reactions, specifically the deprotonation of water molecules ligating the chromium ions [5], Reaction 16:

$$[Cr(H_2O)_6]^{3+} \leftrightarrow [Cr(H_2O)_5OH]^{2+} + H^+$$
 (16)

and perhaps even further:

$$[Cr(H_2O)_5OH]^{2+} \leftrightarrow [Cr(H_2O)_4(OH)_2]^+ + H^+$$
 (17)

$$[Cr(H_2O)_4(OH)_2]^+ \leftrightarrow [Cr(H_2O)_3(OH)_3]^0 + H^+$$
 (18)

The hydroxide ions remaining within the chromium complex structure can serve as bridges, forming connections between adjacent complexes, Reaction 19 ("µ" indicating a bridging ligand) [21,22]:

$$\left[\text{Cr}(\text{H}_2\text{O})_6\right]^{3+} + \left[\text{Cr}(\text{H}_2\text{O})_5\text{OH}\right]^{2+} \leftrightarrow \left[\text{Cr}_2(\text{H}_2\text{O})_{10}(\mu - \text{OH})\right]^{5+} + \text{H}_2\text{O}$$
 (19)

As it was discussed in the introduction section, this phenomenon initiates a reaction known as oligomerization, during which chromium complexes aggregate into charged clusters like dimers  $\left[ \text{Cr}_2(\text{H}_2\text{O})_x(\text{OH})_2 \right]^{4+}, \ \left[ \text{Cr}_2(\text{H}_2\text{O})_y(\text{OH})_3 \right]^{3+}, \ \left[ \text{Cr}_2(\text{H}_2\text{O})_z(\text{OH})_4 \right]^{2+}, \ \text{trimers} \\ \left[ \text{Cr}_3(\text{H}_2\text{O})_9(\text{OH})_4 \right]^{5+}, \ \text{tetramers} \ \left[ \text{Cr}_4\text{O}(\text{H}_2\text{O})_{10}(\text{OH})_5 \right]^{5+}, \ \left[ \text{Cr}_4(\text{H}_2\text{O})_{10}(\text{OH})_6 \right]^{6+} \ \text{or even larger polymers} \ [8,9,23-26]. \ \text{Neutral versions of these compounds then precipitate on the electrode surface} \ [12].$ 

To study this phenomenon further, and to identify how it depends on the negative vertex potential (whose increasingly negative value will generate an increasingly higher local pH), a series of cyclic voltammetry (CV) tests was conducted across various potential windows, as shown in Fig. 2. The 1 mM  $\rm Cr^{3+}$  concentration was selected because the peaks are more prominent at this concentration.

In agreement with Fig. 1, in the blank solution, there is a reduction peak around -0.3 V, as a result of the HER due to proton reduction (Reaction 3a). With more negative applied potentials, proton mass transport becomes the rate-determining step [18]. At approximately -0.8 V, the water reduction reaction (Reaction 3b) starts. In the presence of Cr(III) cations, there is second reduction peak at -0.5 V, which we ascribe to proton release from Cr(III) related acid-base reactions, reactions 16-18, i.e. the deprotonation of water ligands of Cr(III) complexes. If the negative vertex potential is -0.4 V, the cathodic current in the positive-going scan is lower in a way that corresponds to a growing diffusion layer. However, for vertex potentials more negative than ca. -0.5 V, the current in returning positive-going scan becomes very low. For a negative vertex potential of -0.95 V, the current in the reverse scan hardly recovers. This strongly suggests that a layer deposits or precipitates on the gold surface, presumably related to the oligomer formation described above. Additionally, in the reverse scan, some of

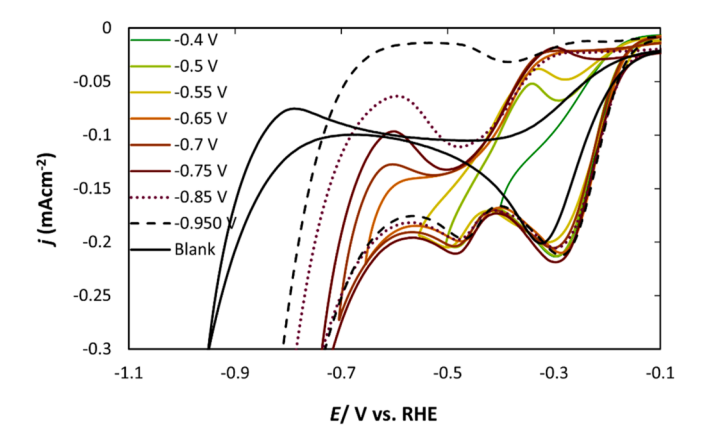


Fig. 2. Cyclic voltammograms (first cycle) of polycrystalline gold electrode at different negative vertex potentials from 0 to -1.2 V for 1 mM Cr(III) solution, pH=2.5 and scan rate=0.005Vs<sup>-1</sup>.

the chromium species related to the precipitate desorb again from the surface, as a result of which the electrode surface is again exposed to the electrolyte and HER from free protons increases the cathodic current. This would explain the cathodic peak in the reverse scan. The effect is less for a vertex potential of -0.95 V, suggesting the formation of the film is more irreversible.

#### 3.2. EQCM measurements

Fig. 3 illustrates the cyclic voltammetry curve (black line) together with the mass changes (red line) of the gold crystal oscillator measured in 0, 0.1, 1, 10, and 100 mM Cr(III) solutions. The pH was maintained at 2.5, the scan rate was 0.005 V/s, and the potential range was from 0 V to -0.75 V. The CVs in Fig. 3 are very similar to those shown in Fig. 1. In the blank without  ${\rm Cr}^{3+}$  in solution (Fig. 5a), the change in the mass of the crystal is minimal, meaning that proton reduction on the gold electrode does not lead to any significant mass change.

With an increase in Cr3+ concentration from 0.1 to 100 mM, considerable mass changes are detected, starting from -0.4 V in the most dilute solution (0.1 mM, Fig. 5b). With the increase in the concentration of Cr(III) cations, the potential at which mass change starts becomes more negative. We relate this potential to the beginning of the deposition/precipitation of the Cr-oxy-hydroxide layer on the gold electrode. For concentrations of 0.1, 1, 10, and 100 mM, this potential shifts from ca. -0.4 to -0.44, -0.5, and -0.68 V, respectively. This observation of an increasingly negative potential for layer deposition with increasing Cr(III) concentration could be linked to their increased buffering strength, suppressing local pH changes. It is worth noting that a pH of 2.5 means that the concentration of protons is 3 mM, so a Cr(III) concentration of 1 mM is anticipated to have a notable effect on the buffering capacity. At potentials where water reduction becomes the dominant reduction reaction, the rate of the mass change first increases and then decreases until it reaches zero, at least for 0.1, 1 and 10 mM Cr (III). Apparently, at some point, the growth of the film stops. For the 100 mM Cr(III) solution, the deposition continues, in the potential window considered, even though water reduction is very dominant under these conditions (considering the high current).

Interestingly, for all Cr(III) concentrations, the mass increase continues or picks up again in the positive-going return scan. Since the HER current is lower in the positive-going scan, the interfacial pH is likely to decrease again, until it reaches a value where the film continues to grow. These observations suggest that the growth of the film is correlated to the local interfacial pH. For low Cr(III) concentrations, the buffering capacity is relatively low and the local pH may quickly reach a value for which the film stops growing. In the return scan, the pH recovers and as a result, the film continues growing. For 100 mM Cr(III), this critical interfacial pH is apparently never reached, and hence the film continues growing. On the other hand, for the other Cr(III) concentrations, the film starts to dissolve at the most positive potentials. This situation is not reached for 100 mM Cr(III), suggesting the formation of a more irreversible/insoluble film under these conditions. Importantly, given the fact that the current is almost entirely due to HER, we assume that film formation itself is non-Faradaic, i.e. there is no reduction of Cr(III) itself. Therefore, there is no direct relationship between charge or current and the observed mass changes, as has been observed in other electrodeposition processes [27]. Future experiments capable of detecting in situ the Cr oxidation states in the film will have to confirm whether there is truly no Cr(II) or Cr(s) formed under the conditions of our experiment.

We also repeated the experiment of opening the potential window in Fig. 2 using EQCM, to monitor the impact of the applied potential on the mass change. Fig. 4 presents the EQCM-CV results for seven different negative vertex potentials, for 1 mM BCS, pH=2.5, and a scan rate of 0.005 V/s. Below -0.4 V, no change in electrode mass occurs, indicating the region where only the HER due to proton reduction takes place. For a negative vertex potential of -0.5 V, we observed an increase in mass from around -0.41 V. During the positive-going sweep, the mass

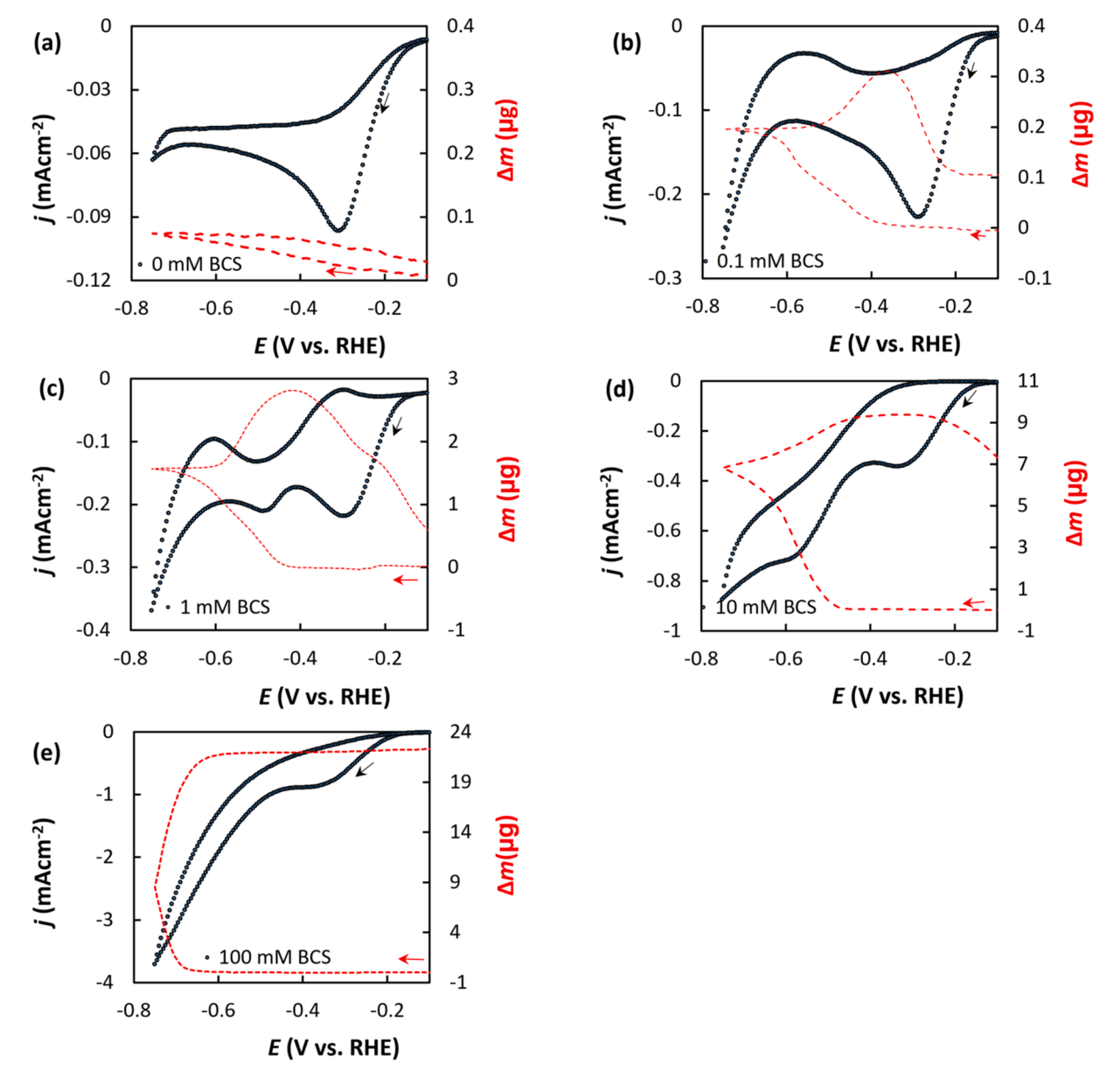


Fig. 3. Simultaneous measurement of the change in the mass of the Au-covered quartz crystal and cyclic voltammogram (first cycle) in different concentrations of Cr (III) cations, pH=2.5 on polycrystalline gold electrode a) Blank b) 0.1 mM c) 1 mM d) 10 mM c) 100 mM Cr(III), scan rate 0.005 Vs<sup>-1</sup>.

continued to increase until -0.4 V, after which it decreased to around zero. In other words, the formation of the deposit is reversible: it forms and then, as the local pH decreases, the deposit dissolves again. The potential of -0.4 V corresponds to the second cathodic peak in the CV which we ascribed to deprotonation of Cr(III) complexes (see Figs. 1 and 2 and their discussion). Deprotonation initiates the oligomerization of Cr (III) complexes, which adsorb on the surface leading to the observed mass increase. In the positive-going reverse scan, the adsorption of complexes continues until -0.4 V and with more positive applied potential the desorption and partial dissolution happens, freeing the surface, so that the HER leads to the cathodic peak in reverse scan. At a negative vertex potential of -0.55 V, a similar trend was observed. When the negative vertex potential was set to -0.65 V, the third cathodic wave due to water reduction starts and in the mass change curves, the rate of mass increase reduces. As mentioned above, we ascribe this termination of the film growth to a critical value of local interfacial pH at which apparently film growth stops. The same termination of film growth is also observed for the other more negative vertex potentials. In addition, when the negative vertex potential is set to  $-0.65~\rm V$  or more negative potentials, the final mass of the deposit at  $-0.10~\rm V$  increases, indicating that as the absolute value of the applied potential increases, the nature of the deposit changes in such a way that it becomes more stable. Even at a bulk pH of 2.5, it remains stable and does not dissolve. Finally, a plot showing how the current and mass change during successive cycles is shown in Fig.S2. It shows the ability of the film to continue growing during successive cycles, but in all cases a plateau in mass is observed within a single cycle.

# 3.3. EC-STM measurements

We conducted in-situ electrochemical scanning tunneling microscopy (EC-STM) measurements to image the microscopic features of Croxy-hydroxide deposition and its correlation with electrochemical measurements. Fig. 5 shows the EC-STM images of Au(111) surface within a  $0.25\mu m \times 0.25\mu m$  area after running several cycles of cyclic voltammetry at different potential windows to monitor the initiation and growth of the Cr-oxy-hydroxide film when the most negative applied potential gradually changes. It is important to stress that all

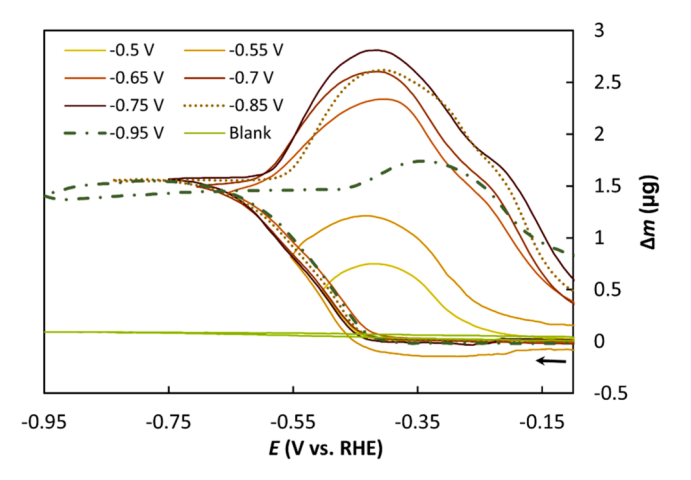


Fig. 4. EQCM mass changes of polycrystalline gold electrode during cyclic voltammetry (first cycle) with increasingly negative vertex potential in 1 mM Cr (III) solution, pH=2.5.

images are taken at 0 V, as no stable images can be obtained at more negative potentials. Fig. 5a shows the image of the pristine Au(111) surface just after thermal annealing at 0 V. Initially, a large terrace with a stripe reconstruction pattern of Au(111) is observed [28], with one long clear step line in the left side of the image. Upon running one CV from 0 to -0.3 V range, some portions of the reconstruction stripes become obscured and some areas with different heights formed on the main terrace, possibly indicating surface adsorption to some extent [29] (Fig. 5b). Since no adatom islands appear, it can be inferred that no deposition has occurred yet, only adsorption. As discussed earlier, no mass change was recorded on the electrode surface during EQCM experiments within this potential window, aligning well with EC-STM observations. Following the second cycle in the 0 to -0.4 V range, the Au stripes are no longer visible and the regions with different heights becomes more visible, yet no deposition or atomic-layer growth is detected on the surface (Fig. 5c). Subsequently, with the third cycle in the 0 to -0.5 V range, a few small islands begin to emerge at the indicated areas in Fig. 5d. Within the potential window of 0 to -0.6 V and 0 to -0.7 V, these small deposited islands evolve into larger clusters, and many new islands have nucleated (Fig. 5e and f). Upon increasing the potential to -0.9 V, the entire area of the terrace becomes covered with deposited clusters (Fig. 5g). At the end of the experiment, when we

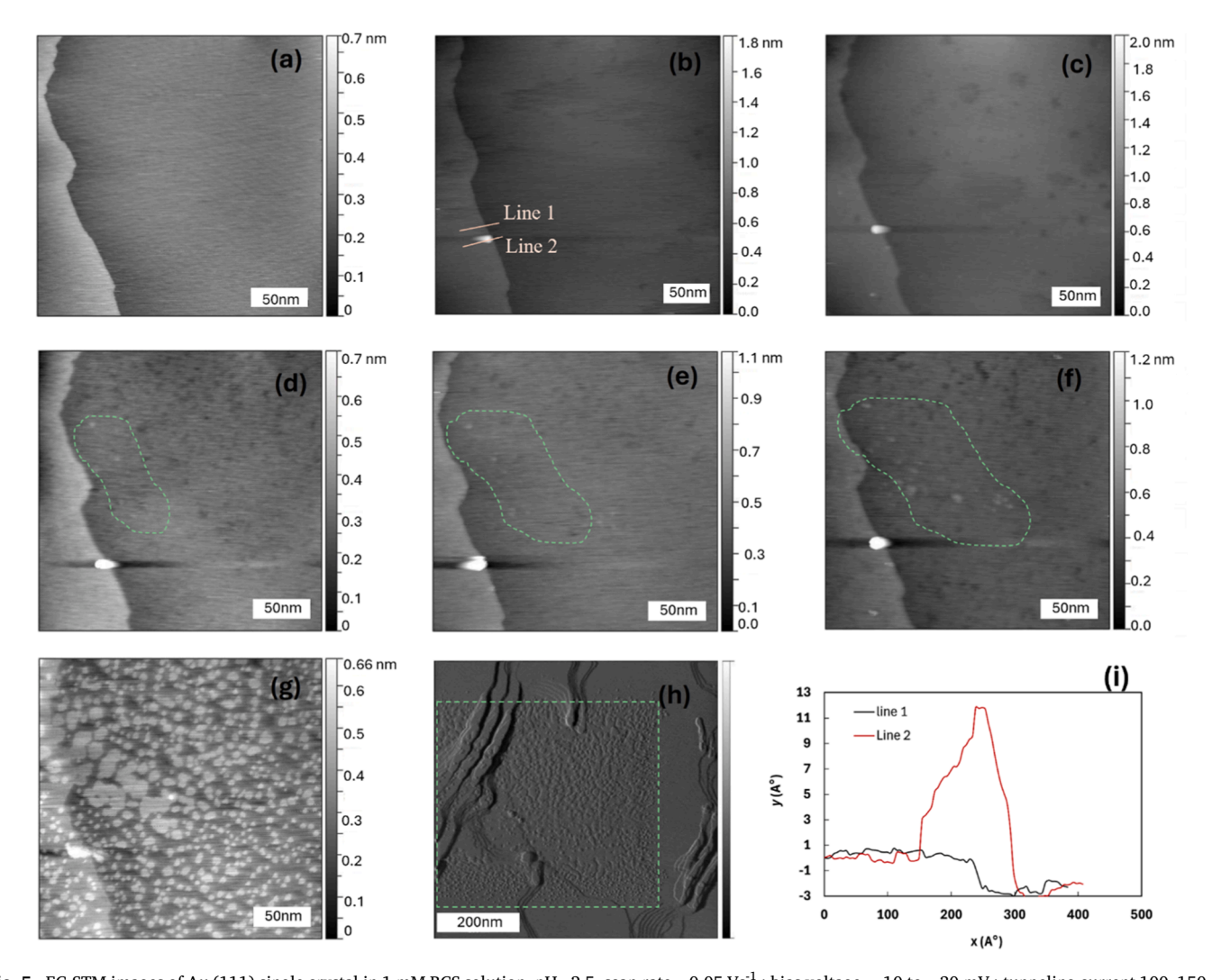


Fig. 5. EC-STM images of Au (111) single crystal in 1 mM BCS solution, pH=2.5, scan rate=  $0.05 \, \text{Vs}^{-1}$ ; bias voltage,  $-10 \, \text{to} -30 \, \text{mV}$ ; tunneling current  $100-150 \, \text{pA}$ . a) before starting the experiment b) after first CV from 0 to  $-0.3 \, \text{V}$  c) after second CV from 0 to  $-0.4 \, \text{V}$  d) after third CV from 0 to  $-0.5 \, \text{V}$  e) after fourth CV from 0 to  $-0.6 \, \text{V}$  f) after fifth CV from 0 to  $-0.7 \, \text{V}$  g) after sixth CV from 0 to  $-0.9 \, \text{V}$  h) zoomed out 3D image of the surface after the last CV from 0 to  $-0.9 \, \text{V}$ , showing the scanned area. (A protrusion next to the step line suddenly has appeared, which could be a contamination particle (based on its height of many atomic steps) that has sticked to the surface i) height line showing the presence of a contamination particle profile, compared to the step edge of image (b).

zoomed out slightly, we observed that the deposition had occurred only in the area scanned by the probe. The corresponding image, clearly showing the scanned area, is shown in Fig. 5h. One possibility for this observation could be that the presence of the probe locally changed the interface conditions, more precisely the local pH, leading to island formation and growth. A similar blockage of diffusion and mass transport, enhancing local pH changes, has been observed in experiments using micro-electrodes [30]. More detailed experiments will be needed to explain the detailed reasons for such local deposition phenomena during the EC-STM experiments.

#### 4. Conclusion

In this paper, we have studied the electrochemical and surface aspects of the cathodic formation of a Cr(III)-based oxy-hydroxide film on a gold substrate. The main electrochemical reaction during electrodeposition of a Cr(III) oxy-hydroxide film from basic chromium (III) sulfate solution with a bulk pH of 2.5, is the hydrogen evolution reaction, either through proton reduction or water reduction. During the cathodic polarization, the local pH becomes more alkaline. This initiates the deprotonation of the hydration shells of the chromium (III) ions. This buffers the local pH but also leads to the oligomerization of the Cr(III) complexes, eventually leading to the precipitation of the chromiumoxyhydroxide film. From EQCM measurements we conclude that there is a specific pH range in which this film grows. At lower pH, the film dissolves; at higher pH, the film growth stops. We also observed that with an increasing Cr(III) concentration or a more negative potential, the deposit changes irreversibly to form an insoluble Cr-oxy-hydroxide film. These are two key aspects of film growth and formation that have not been elucidated as such before, but which clearly follow from our EQCM measurements. EC-STM images confirm the formation of a surface layer with an increasingly negative potential. The STM probe actually enhances the film formation locally on the surface, which we tentatively ascribe to the enhanced pH gradient near the probe.

## CRediT authorship contribution statement

Zahra Sharifi: Writing – original draft, Methodology, Investigation, Formal analysis, Data curation, Conceptualization. Saeid Behjati: Methodology, Investigation, Data curation. Jacques H.O.J. Wijenberg: Writing – review & editing, Supervision, Funding acquisition, Conceptualization. Arnoud C.A. de Vooys: Writing – review & editing, Supervision, Funding acquisition, Conceptualization. Marc T.M. Koper: Writing – review & editing, Supervision, Funding acquisition, Formal analysis, Conceptualization.

## Declaration of competing interest

The authors declare that they have no known competing financial interests or personal relationships that could have appeared to influence the work reported in this paper.

# Acknowledgments

This research was sponsored by Tata Steel Nederland Technology B. V. through the Materials Innovation Institute M2i and the Technology Foundation TTW, which is the applied science division of the Dutch Research Council (NWO) and the Technology Program the Ministry of Economic Affairs of the Netherlands. The research also received support of TOP grant project number 716.017.001, financed by the Dutch Research Council (NWO).

#### Supplementary materials

Supplementary material associated with this article can be found, in the online version, at doi:10.1016/j.electacta.2024.145451.

#### Data availability

Data will be made available on request.

#### References

- R. Giovanardi, G. Orlando, Chromium electrodeposition from Cr (III) aqueous solutions, Surf. Coat. Technol. 205 (15) (2011) 3947–3955.
- [2] V. Protsenko, F. Danilov, Chromium electroplating from trivalent chromium baths as an environmentally friendly alternative to hazardous hexavalent chromium baths: comparative study on advantages and disadvantages, Clean. Technol. Environ. Policy 16 (2014) 1201–1206.
- [3] D. Del Pianta, et al., Determination of the chromium (III) reduction mechanism during chromium electroplating, Electrochim. Acta 284 (2018) 234–241.
- [4] A. Baral, R. Engelken, Modeling, optimization, and comparative analysis of trivalent chromium electrodeposition from aqueous glycine and formic acid baths, J. Electrochem. Soc. 152 (7) (2005) C504.
- [5] V. Bakanov, N. Nesterova, A. Yakupov, Features of electroplating of nanocrystalline chromium coatings from electrolytes based on Cr (III), Protect. Metals Phys. Chem. Surf. 53 (2017) 426–432.
- [6] A. Dasque, et al., Fabrication of a pH microsensor for local pH measurement during chromium electrodeposition from a trivalent chromium-based electrolyte, Electrochem. Commun. 135 (2022) 107213.
- [7] A. Survila, Electrochemistry of Metal complexes: Applications from Electroplating to Oxide Layer Formation, John Wiley & Sons, 2015.
- [8] H. Stuenzi, et al., Early stages of the hydrolysis of chromium (III) in aqueous solution. 4. The stability constants of the hydrolytic dimer, trimer, and tetramer at 25. degree. C and I= 1.0 M, Inorg. Chem. 28 (1) (1989) 66–71.
- [9] F.P. Rotzinger, H. Stuenzi, W. Marty, Early stages of the hydrolysis of chromium (III) in aqueous solution. 3. Kinetics of dimerization of the deprotonated aqua ion, Inorg. Chem. 25 (4) (1986) 489–495.
- [10] J. Wijenberg, et al., Electrodeposition of mixed chromium metal-carbide-oxide coatings from a trivalent chromium-formate electrolyte without a buffering agent, Electrochim. Acta 173 (2015) 819–826.
- [11] F. Danilov, V. Protsenko, Kinetics and mechanism of chromium electroplating from Cr (III) baths. Protect. Metals 37 (2001) 223–228.
- [12] V. Protsenko, T. Butyrina, F. Danilov, Applying a theory of generalized variables to electrochemical kinetics: interpreting the results of studying chromium deposition from Cr (III) baths, Protect. Metals 43 (4) (2007).
- [13] J. Manoj Prabhakar, A. de Vooys, M. Rohwerder, In situ microscopic investigation of ion migration on the surface of chromium coated steels, Npj. Mater. Degrad. 6 (1) (2022) 76.
- [14] J.E. Edy, et al., Kinetics of corrosion-driven cathodic disbondment on organic coated trivalent chromium metal-oxide-carbide coatings on steel, Corros. Sci. 157 (2019) 51–61.
- [15] V. Muralidharan, Critical review on electrochemical quartz crystal micro balanceprinciples and applications to corrosion research, Bull. Electrochem. 17 (4) (2001) 183–192.
- [16] S. Behjati, M.T. Koper, In Situ STM study of roughening of Au (111) single-crystal electrode in sulfuric acid solution during oxidation-reduction cycles, J. Phys. Chem. C 128 (2024) 19024–19034.
- [17] S. Rebouillat, M. Lyons, T. Bannon, Evaluation of the proton transfer kinetics of potential electrolytes in non-aqueous solutions using electrochemical techniques Part 1. Kinetic analysis of the general CE mechanism at stationary and rotating electrodes, J. Solid State Electrochem. 3 (1999) 215–230.
- [18] M.C. Monteiro, et al., The role of cation acidity on the competition between hydrogen evolution and CO2 reduction on gold electrodes, J. Am. Chem. Soc. 144 (4) (2021) 1589–1602.
- [19] A. Goyal, M.T. Koper, The interrelated effect of cations and electrolyte pH on the hydrogen evolution reaction on gold electrodes in alkaline media, Angew. Chem. Int. Ed. 60 (24) (2021) 13452–13462.
- [20] S. Ringe, Cation effects on electrocatalytic reduction processes at the example of the hydrogen evolution reaction, Curr. Opin. Electrochem. 39 (2023) 101268.
- [21] H. Zhao, et al., Mechanism of chromium electrodeposition from Cr (III) baths on nickel and chromium electrode surfaces, Int. J. Electrochem. Sci. 15 (9) (2020) 8979–8989
- [22] A. Haim, Mechanisms of electron transfer reactions: the bridged activated complex, Prog. Inorganic Chem. 30 (1983) 273–357.
- 23] V. Meinhold, et al., Influence of the current regime during electrodeposition in a Cr (III)-containing Fe-Cr-Ni electrolyte on the near-surface pH, alloy composition, and microcrack behavior, Coatings 12 (10) (2022) 1569.
- [24] J.R. Rao, et al., Chromium (III) hydrolytic oligomers: their relevance to protein binding, Biochimica et Biophysica Acta (BBA) 1472 (3) (1999) 595–602.
- [25] H. Stunzi, F.P. Rotzinger, W. Marty, Early stages of the hydrolysis of chromium (III) in aqueous solution. 2. Kinetics and mechanism of the interconversion between two tetrameric species, Inorg. Chem. 23 (14) (1984) 2160–2164.
- [26] H. Stuenzi, W. Marty, Early stages of the hydrolysis of chromium (III) in aqueous solution. 1. Characterization of a tetrameric species, Inorg. Chem. 22 (15) (1983) 2145–2150.
- [27] J. Agrisuelas, et al., An electromechanical perspective on the metal/solution interfacial region during the metallic zinc electrodeposition, Electrochim. Acta 54 (25) (2009) 6046–6052.

- [28] D.J. Trevor, C.E. Chidsey, D.N. Loiacono, In situ scanning-tunneling-microscope observation of roughening, annealing, and dissolution of gold (111) in an electrochemical cell, Phys. Rev. Lett. 62 (8) (1989) 929.

  [29] V. Maurice, H.-H. Strehblow, P. Marcus, In situ STM study of the initial stages of oxidation of Cu (111) in aqueous solution, Surf. Sci. 458 (1–3) (2000) 185–194.
- [30] M.C. Monteiro, et al., Time-resolved local pH measurements during CO2 reduction using scanning electrochemical microscopy: buffering and tip effects, JACS. Au 1 (11) (2021) 1915–1924.